THE PUBLISHING HOUSE
OF THE ROMANIAN ACADEMY

PROCEEDINGS OF THE ROMANIAN ACADEMY, Series A,
Volume 22, Number 2/2021, pp. 185–193

DESIGN AND TESTING A MAGNETO-RHEOLOGICAL BRAKE WITH CYLINDRICAL CONFIGURATION

Raul Alexandru SZAKAL[1], Darius MECEA[1], Alin Ilie BOSIOC[1], István BORBÁTH[2], Sebastian MUNTEAN[3]

[1] University Politehnica of Timişoara, Bd. Mihai Viteazu 1, RO-300222, Timişoara
[2] ROSEAL S.A., Str. Nicolae Balcescu, 5A, RO-535600, Odorheiu Secuiesc
[3] Romanian Academy – Timişoara Branch, Bd. Mihai Viteazu 24, RO-300223, Timişoara

Corresponding author: Sebastian MUNTEAN, E-mail: seby@acad-tim.tm.edu.ro

Abstract. The paper focuses on design considerations and experimental investigations of a MRB with cylindrical configuration. The design considerations for MRB with cylindrical configuration are presented. The magneto-rheological torque contribution is estimated at the design stage based on geometric configuration and the proprieties of the magneto-rheological fluid (MRF132DG) selected for this case. The MRB is manufactured and investigated on a range of speeds from 100 rpm to 1100 rpm for voltage values applied to the coil up to 32V. The mechanical, electromagnetic and magneto-rheological contributions are discriminated from the braking torque assessing the performances of the MRB. The variation in time of the torque under different speed values and several voltages applied to the coil is investigated in order to explore the MRB response time. The design methodology is validated against the data determined on MRB configuration. The conclusions on the design methodology of MRB and its operation are underlined in last section.

***Key words**:* magneto-rheological brake, design, experimental investigations, performance assessment.

1. INTRODUCTION

The magneto-rheological devices are widely used in application such as magneto-rheological dampers [1–4], brakes [5–8], clutches [9], shock absorbers [10] and gas rotating gaskets [11]. The magneto-rheological brakes (MRBs) slow down the speed of a rotating shaft immersed in the magneto-rheological fluid (MRF). The braking torque strongly depends on the MRB geometry [12]. The disc-type MRBs are used in a wide range of applications. The drum-type MRBs convert the MR effect in braking torque with lower inertia compared to disc MRBs [13]. The analysis performed on a single disc MRB and on a single drum MRB highlighted the interdependence of the measures of performance as a function of the dimensions [14]. The results have demonstrated that both MRBs are equivalent in terms of torque density but drum MRBs are more reactive and require less power. The MRB with cylindrical configuration is similar with the drum one. However, the cylindrical-type can be selected for particular geometrical configurations. MRB works in shear mode while its performances depend on: (i) clearance gap, (ii) working speed, (iii) magnetic field strength, and (iv) effective area, respectively. The methodology developed to design MRB with cylindrical configuration is based on estimating the quantities listed above and taking into account specific geometrical constrains.

The paper focuses on design considerations and experimental investigations of a MRB with cylindrical configuration. The design considerations for MRB with cylindrical configuration are detailed in Section 2. The magneto-rheological torque contribution is estimated at the design stage based on geometric configuration and the proprieties of the magneto-rheological fluid (MRF) selected for this case. A commercial MRF132DG provided by Lord Co. is considered in these investigations. Next section provides the experimental results obtained at several speeds with MRB using MRF132DG. The MRB is manufactured and investigated on a range of speeds from 100 rpm to 1100 rpm for voltage values applied to the coil up to 32V. The design methodology is validated against experimental data determined on MRB with cylindrical configuration. The results predicted by the design methodology are compared against experimental data. The

conclusions on the design methodology of the MRB with cylindrical configuration and its performances determined on test rig are underlined in last section.

2. DESIGN A MRB WITH CYLINDRICAL CONFIGURATION

The first step in designing the MRB is to select the type. This stage starts from the geometric space available for MRB with a length of $L = 60$ mm and outer radius of $R_{ext} = 40$ mm, respectively. A volume of 267 cm^3 is available for MRB taking into account the inner radius of $R_{int} = 13.5$ mm, Fig. 1. The R_{ext}/L ratio of 0.67 is obtained for our configuration. The disc-type MRB is the most common design due to it is easy to manufacture and leads to reasonably good results in terms of weight and compactness [15]. However, the geometrical criterion $R_{ext}/L < 0.36$ for this type is not fulfilled in our case. Neither T-type MRB ($R_{ext}/L > 1.5$) nor T-type MRB with two-coil hybrid configuration ($0.75 < R_{ext}/L < 1.5$) are applicable in this case. The drum-type MRB is out of selection because the ratio has to be grater than 2 ($R_{ext}/L > 2$). A single-coil hybrid configuration of MRB is recommended by Nguyen and Choi [15] for the geometry ratio $0.36 < R_{ext}/L < 0.75$. In our case, we have selected a MRB with cylindrical configuration and single-coil, respectively.

The design requirement for MRB device is a braking torque of 5.5 Nm at speed of 800 rpm yielding a braking power of 460 W. The main parts of the MRB device are following: (1) magneto-rheological fluid (MRF) and (2) magnetic circuit including the coil and magnetic house, respectively. The coil is designed to ensure magnetic flux taking into account the geometric constraints imposed by its arrangement at the bottom of the MRB. The magnetic house is manufactured by soft iron and it is designed to guide the magnetic flux to the clearance gap filled with MRF. The rotating part is the cylindrical geometry together with the shaft (marked with green in Fig. 2). MRF volume around 20 ml is used in our MRB device.

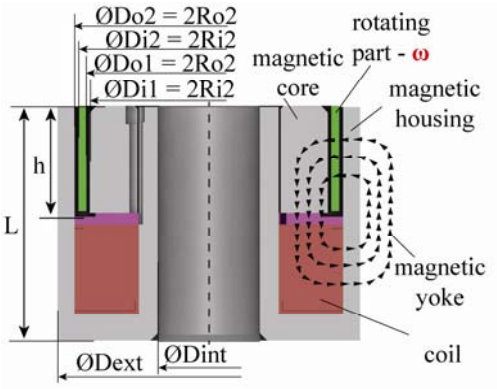

Fig. 1 – MRB with cylindrical configuration.

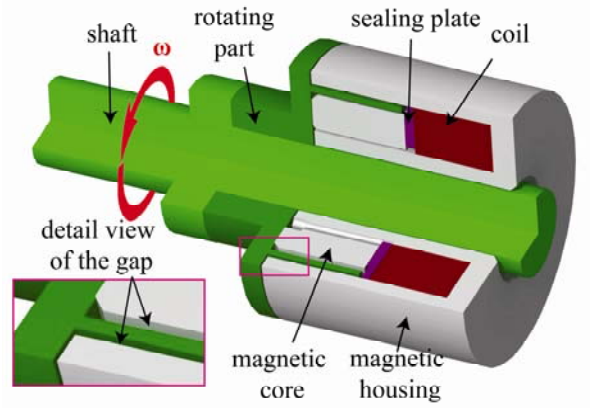

Fig. 2 – Axonometric view of MRB. The rotating part includes the cylindrical geometry and the shaft colored with green.

The power (P_{MR}) required in the braking process is estimated at the design stage exclusively on magneto-rheological mechanisms neglecting other mechanical and electromagnetic contributions. The magneto-rheological torque (T_{MR}) is estimated at the design stage based on equation developed for cylinder rotational viscometer given by equation (2) for power law non-Newtonian fluid model. The laminar flow of the incompressible non-Newtonian fluid under constant angular speed (ω) are the assumptions considered for equations (2) applied to Searle systems where the cylindrical part rotates together with the shaft and the casing is stationary [16, 17]:

$$P_{MR} = T_{MR}\ \omega \tag{1}$$

$$T_{MR} = 2\pi h R_{i2}^2 \left(\frac{2\omega}{m}\right)^2 c\left[1-\left(\frac{R_{i2}}{R_{o2}}\right)^{\frac{2}{m}}\right]^{-m} + 2\pi h R_{o1}^2 \left(\frac{2\omega}{m}\right)^2 c\left[1-\left(\frac{R_{o1}}{R_{i1}}\right)^{\frac{2}{m}}\right]^{-m}. \tag{2}$$

Two types of parameters (length of the gap $h = 28$ mm and the radii $R_{o1} = 31.5$ mm, $R_{i1} = 32.5$ mm, $R_{o2} = 34.5$ mm, $R_{i2} = 35.5$ mm) associated with the geometrical configuration and the magneto-rheological proprieties (shear

stress τ [Pa]) of the MRF in terms of the shear strain rate $\dot{\gamma}$ [s^{-1}] (corresponding to the speed of the MRB) and the magnetic flux density B [T] (in the MRF available inside the clearance gap of MRB) are required at the design stage. The geometrical parameters are selected by the designer taking into account constrains imposed by the technical solution.

MRFs belong to an important part of smart materials domain whose rheological properties change rapidly with the magnetic field. In the presence of external magnetic fields, the MRF can change its behaviour and can produce semi-solid state (chain-like structure) from the liquid state within few milliseconds [18, 19]. The experimental investigations performed with MRB using several MRFs have revealed their capabilities [20]. The MRF selected in this application is a commercial MRF132DG provided by Lord Co designed for general use in controllable, energy-dissipating applications such as in MRBs [14, 15, 21]. MRF132DG fluid is a suspension of micron-sized, magnetizable particles in a hydrocarbon carrier fluid with the operating temperature range from –40ºC to 130ºC. The magneto-rheological proprieties of the MRF132DG are available at the design stage based on the experimental investigations [22] performed using Physica MCR 300 rheometer available at University Politehnica Timisoara. The experimental data for the flow curves $\tau(\dot{\gamma})$ and their fits with non-Newtonian power law fluid model (3) are given in Fig. 3

$$\tau(\dot{\gamma}) = c\,\dot{\gamma}^{m}, \tag{3}$$

where c is the coefficient and m is the power exponent of the non-Newtonian power law fluid model. Both parameters (c, m) of the non-Newtonian power law model obtained by fitting the experimental data together with R^2 coefficient are included in Table 1 for several values of the magnetic flux density from 0.05 T to 0.6 T.

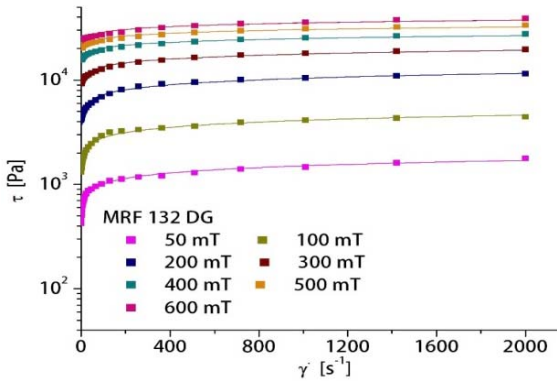

Fig. 3 – Flow curves determined for MRF132DG for several magnetic flux density values from 50 mT to 600 mT.

Table 1

The fit parameters of the non-Newtonian power law model applied on the experimental data given in Fig. 3

B [T]	c	m	R^2
0.05	438.29	0.172	0.9999
0.1	1335.19	0.166	0.9991
0.2	3543.44	0.156	0.997
0.3	7728.13	0.119	0.999
0.4	13198.37	0.09	0.998
0.5	17512.00	0.085	0.9998
0.6	20641.00	0.085	0.999

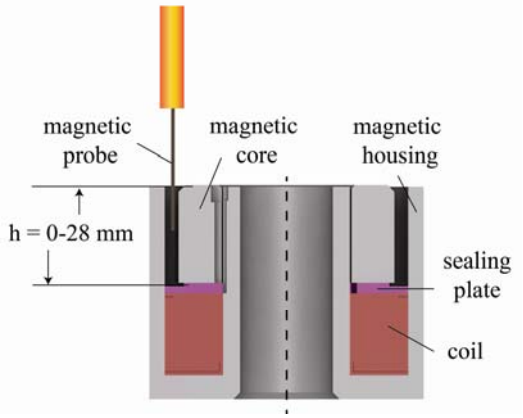

Fig. 4 – Experimental setup to measure the magnetic flux density in the clearance gap of MRB.

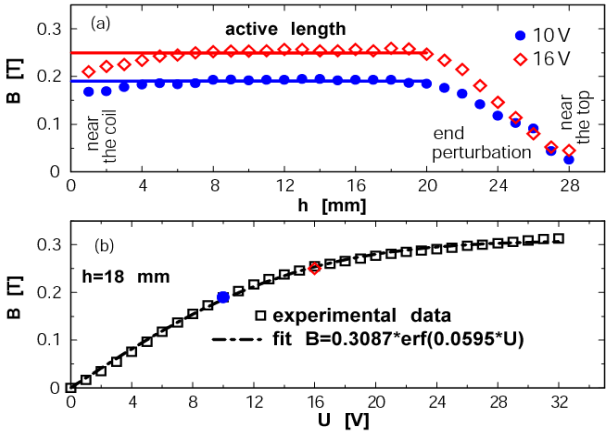

Fig. 5 – a) Magnetic flux density (B) versus voltage (U) at h=18 mm; b) magnetic flux density (B) along the gap length of MRB for two voltage values (10V and 16V) applied to the coil.

The magnetic field induced by the coil in the clearance gap filled with MRF132DG is measured using a FW Bell Hall probe as in Fig. 4. Two types of investigations were carried out in the clearance gap of MRB: (a) the magnetic flux density along the gap is measured. The magnetic flux density along the gap is measured for two voltage values of 10V and 16V applied to the coil. The position near to the coil corresponds to the length value of 0 while the value of 28 mm corresponds to the top side of the MRB (Fig. 4). The magnetic flux density (B) measured along the gap length (h) is plotted in Fig. 5a. One can observe that a constant value of the magnetic flux density is determined along two third length of the gap. Contrary, a significant deviation of the magnetic flux density was identified at the end of the gap (closed to the top from 20 mm to 28 mm), see Fig. 5a. Next, the magnetic flux density is measured on the flat region for the voltage applied to the coil from 0 to 32V with an increment of 1V. The magnetic flux density measured with the probe in the clearance gap at h =18 mm for several values of the voltage applied to the coil is given in Fig. 5b. This data is used to assess the design methodology.

3. INVESTIGATION THE PERFORMANCE OF MRB

The MRB device designed by Timisoara's team was manufactured by ROSEAL S.A. A test rig was designed and developed to assess the performances of the MRB (Fig. 6).

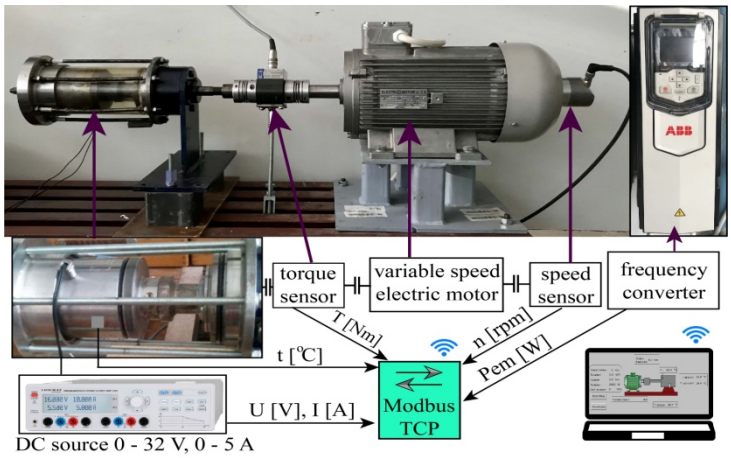

Fig. 6 – Test rig developed to assess MRB's performances available at University Politehnica of Timisoara.

The test rig consists in a variable speed electrical motor controlled by frequency converter, a torque sensor, MRB, DC source and the control and acquisition system implemented on PC using remote control by wireless. The control and acquisition system setup the speed of the electric motor and records the following data: (i) the torque (T [Nm]); (ii) speed (n [rpm]); (iii) power of the electrical motor estimated by the frequency converter P_{em} [W]; (iv) the voltage U [V] and current I [A] applied to the coil; and (v) the temperature (t [°C]), respectively. The temperature is acquired on the inside and outside walls of the MRB with accuracy in limit of ±1.5°C. The temperature inside of the MRB closed to the MRF was below the threshold limit of 80°C during all measurement campaigns. The control software platform is used to setup the speed of the electrical motor from 100 rpm to 1100 rpm with increment of 100 rpm. The control platform is designed to prevent the failure of the torque transducer by imposing the highest threshold value. As a result, the measurement campaign is suddenly completed if the torque threshold value is exceeded during the investigation. Five campaigns are performed to check the repeatability of experimental data. Note that this investigation was performed in air.

The braking torque of the MRB is measured for the voltage values applied to the coil from 2V to 32V at the constant current value of 5A and eleven speed regimes from 100 rpm to 1100 rpm (Fig. 7). The design torque value of 5.5 Nm (light blue line in Fig. 7) at speed of 800 rpm is reached for greater voltage values than 12V. One can remark a logarithmic distribution of the braking torque of the MRB in terms of the speed. The same behavior is revealed for multilayer MRB tested by Rossa et al. [23, Fig. 11]. This distribution of the braking torque with speed regime remains unchanged up to voltage value of 24V. The distribution

changes for the voltage values higher than 24V. The maximum torque of 7.47 Nm is reached at speed of 200 rpm for the voltage value of 32V. However, diminished values of the braking torque are distinguished at large speeds and highest voltage values (i.e. 28V and 32V). A torque density of 28 kN/m^2 is obtained for MRB investigated in this paper. MRB (RD-2078-01) commercially available from Lord Co. has a torque density of 12.5 kN/m^2 according to Senkal and Gurocak [21] and Rossa et al. [23]. It is desirable to design a MRB with a higher torque density but in this case the temperature level has to be carefully controlled.

The maximum braking power determined on the MRB is 0.85 kW (Fig. 8). The linear distribution of the braking power in terms of speed is obtained for all voltages applied to the coil up to 24V. It is assumed that the change in distribution comes from modification of the flow structure due the behavior of the MRF.

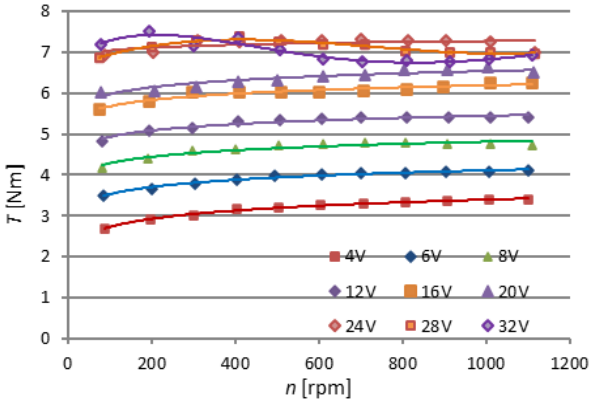

Fig. 7 – Braking torque (T [Nm]) of MRB for voltage values up to 32V over range speed from 100 rpm to 1100 rpm.

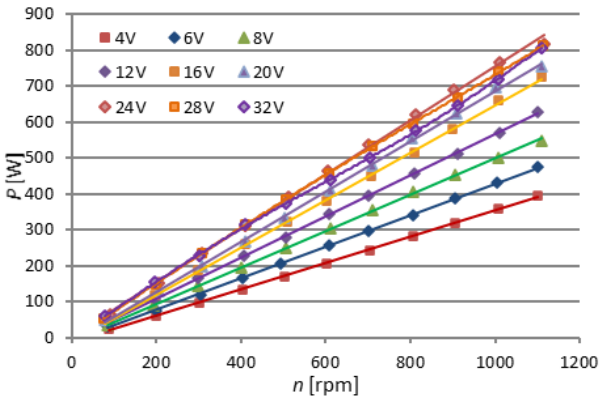

Fig. 8 – Braking power (P [W]) provided by MRB for voltage values up to 32V over range speed from 100 rpm to 1100 rpm.

One reason for this modification of the torque/power distribution could be temperature due to the mechanical load of MRB is dissipated during the braking process in heat. Therefore, the proprieties of the MRF are the key issues in these engineering applications. The temperature acquired on the outside wall of the MRB at each regime speed is plotted in Fig. 9. One can observe that the temperature measured at starting point of each campaign (at the speed of 100 rpm) for different voltages applied to the coil reveals a random evolution. This happened because after each measurement campaign the brake was forced cooled with a fan until the next one started. It can be noticed that the same temperature values are reached for the voltage values of 12V, 28V and 32V applied to coil at high speeds. As a result, temperature is not the only parameter that leads to changes in MRB behavior. This behavior of MRB will be examined in our further investigations. In conclusion, it is recommended that actual MRB to be operated up to the maximum voltage of 24V. In this way, the maximum electrical power consumed by the coil of 160 W is reduced by a quarter, improving the thermal behavior of the MRB.

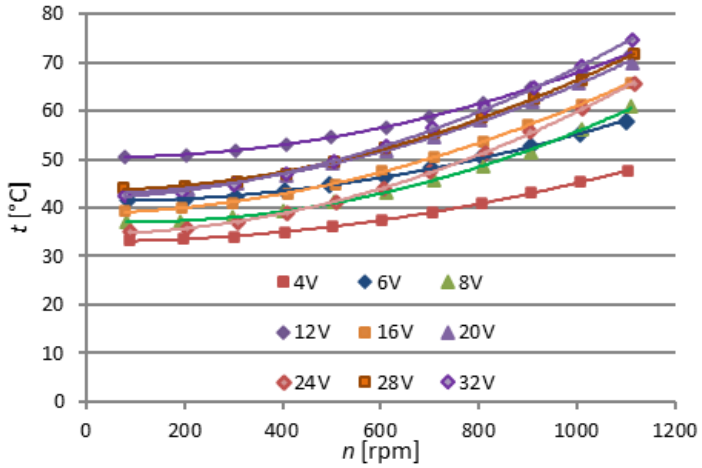

Fig. 9 – Temperature (t [°C]) acquired on the outside wall of the MRB at each speed regime.

The braking torque (T) delivered by MRB includes mechanical (T_{MEC}), electromagnetic (T_{EM}) and magneto-rheological (T_{MR}) contributions. The values of the braking torque provided by MRB change with the speed (n) and the voltage (U) applied to the coil.

$$T(n, U) = T_{MEC}(n) + T_{EM}(n, U) + T_{MR}(n, U). \quad (4)$$

Further investigations are carried out to discriminate the contribution of mechanical, electromagnetic and magneto-rheological parts from the braking torque (T). The first investigation was conducted without MRF in the clearance gap of MRB and without any voltage applied to the coil. The mechanical torque $T_{MEC}(n)$ due to friction in bearing and seals is obtained being marked with black in Fig. 10.

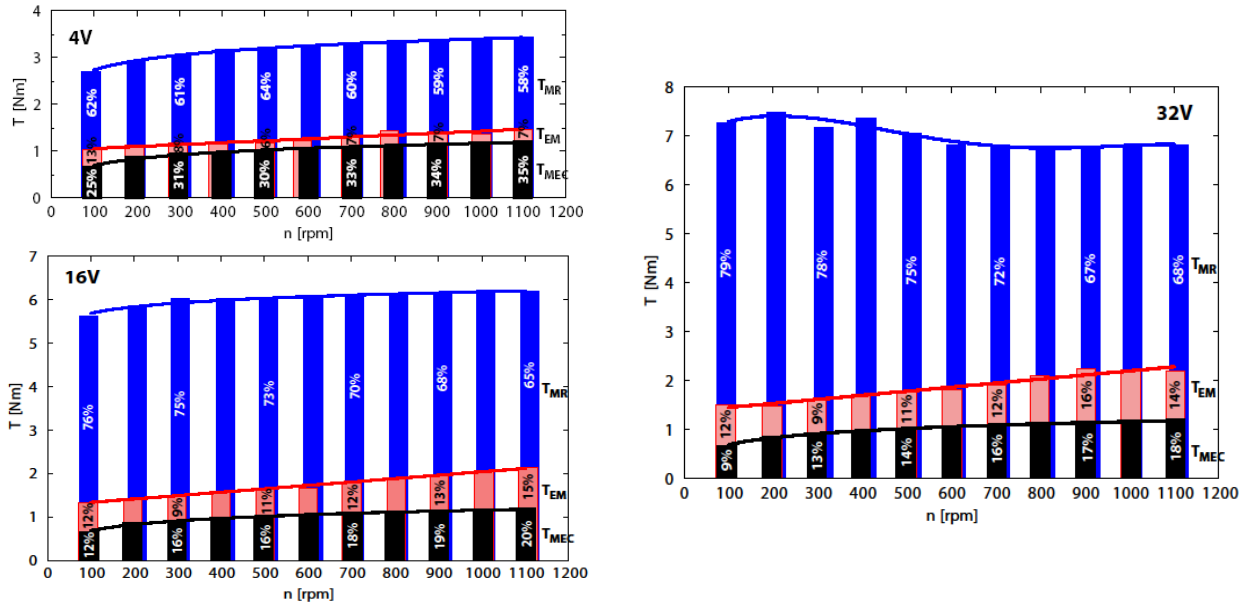

Fig. 10 – Mechanical, electromagnetic and magneto-rheological contributions discriminated from the braking torque of the MRB at 4V (top/left), 16V (bottom/left) and 32V (right).

Then, the voltage values are applied to the coil. Note that investigations are still conducted without the MRF inserted in the clearance gap of MRB. The electromagnetic contribution $T_{EM}(n,U)$ from the total torque is discriminated as the difference between the mechanical value T_{MEC} previously determined and the torque value (T_{MEC}+T_{EM}) measured for the same speeds and different voltage values, respectively. This electromagnetic part is colored with pink in Fig. 10.

Furthermore, the clearance gap of MRB is filled with MRF132DG to which a process of homogenization and elimination of air bubbles has been previously applied. Then, the braking torque $T(n,U)$ measurements are performed for the same speed and voltage values applied to the coil, respectively. As a result, the braking torque delivered by MRB is measured. Then, the magneto-rheological contribution $T_{MR}(n,U)$ is yielded as difference between the braking torque (T) and the values of the torque (T_{MEC}+T_{EM}) measured at the previous stage. The magneto-rheological component is indicated with blue color in Fig. 10. The discriminated contributions of mechanical, electromagnetic and magneto-rheological parts from braking torque (T) are shown in Fig. 10 for three voltage values (i.e. 4V, 16V and 32V) applied to the coil. The mechanical contribution to the braking torque increases with speed, but it remains unchanged under the magnetic field. The mechanical contribution is from 25% at 100 rpm to 35% at 1100 rpm at the voltage of 4V and from 9% at 100 rpm to 18% at 1100 rpm at maximum voltage value of 32V, respectively. It can be concluded that the mechanical part is more significant for larger braking torque values, reaching a maximum of 35% at the highest speed and low voltage values.

It is logical that the electromagnetic contribution to be correlated with the magnetic field induced by the coil. However, one can distinguish an influence of the speed on the electromagnetic part. That can be explained due to the friction induced by the electromagnetic forces in seals. The electromagnetic contribution is in limit of 8% at voltage value of 4V excepting the speed of 100 rpm where this part is 13%. This electromagnetic

contribution reaches a maximum value of 15% at 16V and the highest speed of 1100 rpm. The same distribution of the electromagnetic contribution is found at 32V revealing a saturation of the magnetic field beyond the value of 16V. This statement is supported by the measurement presented in Fig. 5b.

The magneto-rheological contribution covers the range from 58% to 79% of the braking torque. It can be seen that the magneto-rheological contribution decreases from 79% at 100 rpm to 68% at 1100 rpm at a voltage of 32V applied to the coil. The magneto-rheological contribution monotonically decreases with increasing the speed. This tendency corresponds to the shear thinning behavior of the MRF. One can conclude that the magneto-rheological contribution is the most significant for all regimes in correlation with the hypothesis considered at the design stage.

The variation in time of the MRB torque for prescribed speed values from 100 rpm to 1100 rpm with a step of 100 rpm and nine voltages (4V, 6V, 8V, 12V, 16V, 20V, 24V, 28V and 32V) applied to the coil is plotted in Fig. 11. The acquired values of the MRB shaft speed are marked with blue diamond symbol on each plateau of 10 seconds. A closed loop is implemented in our experimental setup to control the speed of the MRB shaft using the ACS850 frequency converter. Therefore, the time variation of the MRB shaft speed is in limit of ± 2%. The time variation of the torque is within ± 4% on each plateau. These results lead to the conclusion that MRB is able to respond quickly over time.

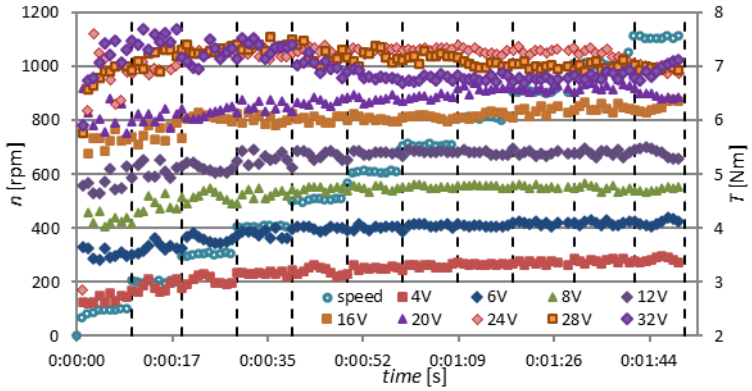

Fig. 11 – Variation in time of the speed and torque of MRB for five voltage values applied to the coil.

4. ASSESSMENT OF THE DESIGN METHODOLOGY

The design methodology developed in section 2 is assessed against experimental data presented in section 3. As expected, larger magneto-rheological contribution is determined at stronger magnetic field corresponding to higher values of the voltage applied to the coil. The magneto-rheological torque (T_{MR}) values for four voltage values of 4V, 8V, 16V and 32V are discriminated from the experimental data in terms of the magnetic flux density at speed of 300 rpm. The experimental data are marked with circles in Fig. 12.

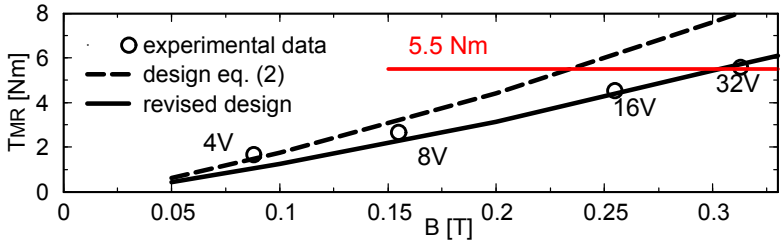

Fig. 12 – Magneto-rheological torque (T_{MR}) *versus* magnetic flux density (B).
Comparison the magneto-rheological torque determined with equation (2) against experimental data.

The magneto-rheological torque (T_{MR}) is estimated at the design stage based on equation (2). The MRB's speed of 300 rpm corresponds to the shear strain rate of $\dot{\gamma} \approx 2\,000\ \mathrm{s}^{-1}$ for the geometrical configuration given in Fig. 1. The magneto-rheological proprieties for MRF132DG are measured up to

maximum shear strain rate value of $\dot{\gamma} \approx 2000\ s^{-1}$ using a rheometer with plate-plate configuration (Fig. 3). The magneto-rheological torque estimated based on equation (2) for MRB with cylindrical configuration and operating with MRF132 DG at 300 rpm is plotted with black dashed line in Fig. 12. The magneto-rheological torque is overestimated for all magnetic flux density values. The magnetic flux density measured along the MRB gap (Fig. 5a) has showed that the active length is only two-thirds of the gap length (h). As a result, the magneto-rheological torque estimated by equation (2) has to be revised with the end correction [16]. The magneto-rheological torque revised taking into account the end correction of the gap's length is plotted in Fig. 12 with black solid line. One can remark that the revised magneto-rheological torque is quite well approximated against experimental data proving the feasibility of the hypothesis embedded in the design methodology.

5. CONCLUSIONS

The design considerations and experimental investigations on a MRB with cylindrical configuration are presented. From the beginning, the technical requirements associated with the MRB device are defined. MRB with cylindrical configuration is selected taking into account both geometrical constrains available in this case and design considerations provided in the literature. The magneto-rheological torque of the MRB is estimated at the design stage based on the geometric configuration and MRF132DG properties. All parts of the MRB with cylindrical configuration are designed. Then, the MRB is manufactured and installed on the test rig. The MRB is investigated on a range of speeds from 100 rpm to 1 100 rpm for voltage values applied to the coil up to 32V. The design torque value of 5.5 Nm at speed of 800 rpm is reached for greater voltage values than 12V. A logarithmic distribution of the braking torque in term of the speed is obtained up to voltage value of 24V. The distribution changes for the voltage values higher than 24V revealing diminished values of the braking torque at large speeds and highest voltage values. The maximum torque of 7.47 Nm is reached at speed of 200 rpm for the voltage value of 32V yielding a torque density of 28 kN/m^2 for MRB investigated in this paper. The linear distributions of the braking power in terms of speed are obtained for voltage values below to 24V. It is recommended that MRB to be operated up to the maximum voltage of 24V in order to keep limited the thermal behavior and the linearity of the power braking, respectively. The mechanical, electromagnetic and magneto-rheological contributions from braking torque are discriminated. The largest contribution is delivered by magneto-rheological part supporting the hypothesis considered at the design stage. The time variation investigations carried out lead to the conclusion that MRB is able to respond quickly over time. Next, the design methodology is validated against the data determined on MRB. The end correction of the active length of the gap proved to be important in more accurate capture of the measured magneto-rheological torque.

ACKNOWLEDGEMENTS

Dr. S. Muntean has been supported by the research programs of Hydrodynamic, Cavitation and Magnetic Liquid Division from Center for Fundamental and Advanced Technical Research, Romanian Academy Timisoara Branch. The authors thank Dr. L. Vékás, corresponding member of the Romanian Academy for his valuable support given in the last decade on MR topic and his suggestions to improve the scientific level of the manuscript.

REFERENCES

1. D.H. WANG, W.H. LIAO, *Magnetorheological fluid dampers: a review of parametric modelling*, Smart Mater. Struct., **20**, p. 023001, 2011.
2. M. LIȚĂ, N. POPA, C. VELESCU, L. VÉKÁS, *Investigations of a magnetorheological fluid damper*, IEEE Trans. Magn., **40**, *2*, pp. 469-472, 2004.
3. N. FILIP-VACARESCU, C. VULCU, D. DUBINĂ, *Numerical study of a hybrid damping system composed of a buckling restrained brace with a magneto rheological damper*, Proc. Romanian Acad. A, **18**, *3*, pp. 273-280, 2017.

4. M. GIUCLEA, T. SIRETEANU, D. STANCIOIU, C.W. STAMMERS, *Modelling of magnetorheological damper dynamic behavior by genetic algorithms based inverse method*, Proc. Romanian Acad. A, **5**, *1*, pp. 55-63, 2004.
5. J.D. CARLSON, D.F. LEROY, J.C. HOLZHEIMER, D.R. PRINDLE, R.H. MARJORAM, *Controllable brake*, US Patent no. 5842547, 1998.
6. J.D. CARLSON, *Magneto-rheological brake with integrated flywheel*, US Patent no. 6186290, 2001.
7. S. MUNTEAN, A.I. BOSIOC, R.A. SZAKAL, L. VÉKÁS, *Hydrodynamic investigation in a swirl generator using a magneto-rheological brake,* In: *Materials Design and Applications* (Ed. L.F.M. Da Silva), Advanced Structured Materials, Springer, Cham, **65**, pp. 209-218, 2017.
8. R.A. SZAKAL, A.I. BOSIOC, S. MUNTEAN, D. SUSAN-RESIGA, L. VÉKÁS, *Experimental investigations of a magneto-rheological brake embedded in a swirl generator apparatus*, In: *Materials Design and Applications II* (Ed. L.F.M. Da Silva), Advanced Structured Materials, Springer, Cham, **98**, pp. 265-279, 2019.
9. A.I. BOSIOC, T. ARDELEAN, R.A. SZAKAL, S. MUNTEAN, I. BORBÁTH, L. VÉKÁS, *Experimental investigations of a MR clutch for a centrifugal pump*, In: *Materials Design and Applications II* (Ed. L.F.M. Da Silva), Advanced Structured Materials, Springer, Cham, **98**, pp. 253-263, 2019.
10. A. MILECKI, M. HAUKE, *Application of magnetorheological fluid in industrial shock absorbers*, Mech. Syst. Sign. Proces., **28**, pp. 528–541, 2012.
11. T. BORBÁTH, D. BICA, I. POTENCZ, I. BORBÁTH, T. BOROS, L. VÉKÁS, *Leakage-free rotating seal systems with magnetic nanofluids and magnetic composite fluids designed for various applications*, Int. J. Fluid Mach. Syst., **4**, *1*, pp. 67-75, 2011.
12. Q.H. NGUYEN, V.T. LANG, S.B. CHOI, *Optimal design and selection of magnetorheological brake types based on braking torque and mass*, Smart Mater. Struct., **24**, p. 067001, 2015.
13. T. KIKUCHI, K. KOBAYASHI, *Development of cylindrical magnetorheological fluid brake for virtual cycling system*, IEEE International Conference on Robotics and Biomimetics (ROBIO), pp. 2547-2552, 2011.
14. C. ROSSA, A. JAEGY, J. LOZADA, A. MICAELLI, *Design considerations for magnetorheological brakes*, IEEE/ASME Trans. on Mechatronics, **19**, *5*, pp. 1669-1680, 2014.
15. Q.H. NGUYEN, S.B. CHOI, *Selection of magnetorheological brake types via optimal design considering maximum torque and constrained volume*, Smart Mater. Struct, **21**, p. 015012, 2012.
16. J.F. STEFFE, *Rheological methods in food process engineering*, 2nd edition, Freeman Press, MI, USA, 1996.
17. J. HUANG, J.Q. ZHANG, Y. YANG, Y.Q. WEI, *Analysis and design of a cylindrical magneto-rheological fluid brake*, J. Mater. Process. Technol., **129**, pp. 559-562, 2002.
18. L. VÉKÁS, *Ferrofluids and magnetorheological fluids*, Adv. Sci. Tech., **54**, pp. 127-136, 2008.
19. R. AHAMED, S.-B. CHOI, M.M. FERDAUS, *A state of art on magneto-rheological materials and their potential applications*, J. Intell. Mater. Syst. Struct., **29**, *10*, pp. 2051-2095, 2018.
20. A.I. BOSIOC, T.E. BEJA, S. MUNTEAN, I. BORBÁTH, L. VÉKÁS, *Experimental investigations of MR fluids in air and water used for brakes and clutches*, In: *Materials Design and Applications* (Ed. L.F.M. Da Silva), Advanced Structured Materials, Springer, Cham, **65**, pp. 197-207, 2017.
21. D. SENKAL, H. GUROCAK, *Serpentine flux path for high torque MRF brakes in haptics applications*, Mechatronics, **20,** pp. 377-383, 2010.
22. D. SUSAN-RESIGA, *A rheological model for magneto-rheological fluids*, J. Inter. Mat. Syst. Str., **20**, *8*, pp. 1001-1010, 2009.
23. C. ROSSA, A. JAEGY, A. MICAELLI, J. LOZADA, *Development of a multilayered wide-range torque magnetorheological brake*, Smart Mater. Struct., **23**, p. 025028, 2014.

Received November 14, 2020